Determination of the optical properties of the human uterus using frequency-domain photon migration and steady-state techniques

1994 Phys. Med. Biol. 39 1191

(http://iopscience.iop.org/0031-9155/39/8/001)

Phys. Med. Biol. 39 (1994) 1191–1202. Printed in the UK

Determination of the optical properties of the human uterus using frequency-domain photon migration and steady-state techniques

Steen J Madsen†, Pius Wyss‡, Lars O Svaasand§, Richard C Haskell‖, Yona Tadir† and Bruce J Tromberg†¶

† Beckman Laser Institute and Medical Clinic, University of California, Irvine, CA 92715, USA

‡ University Hospital of Zurich, 8093 Zurich, Switzerland

§ University of Trondheim, 7000 Trondheim, Norway

‖ Harvey Mudd College, Claremont, CA 91711, USA

Received 8 March 1994

Abstract. The optical properties (absorption and transport scattering coefficients) of freshly excised, bulk human uterine tissues were measured at 630 nm using frequency-domain and steady-state photon migration techniques. Measurements were made on both normal (pre- and post-menopausal) and non-neoplastic fibrotic tissues. The absorption coefficient of normal post-menopausal tissue (~ 0.06 mm^{-1}) was found to be significantly greater than that of normal pre-menopausal tissue (0.02–0.03 mm^{-1}) and pre-menopausal fibrotic tissue (0.008 mm^{-1}). The transport scattering coefficient was similar in all three tissue types considered (0.6–0.9 mm^{-1}).

From the preliminary results presented here, we conclude that optical properties can be reliably calculated either from the frequency-dependent behaviour of diffusely propagating photon density waves or by combining the frequency-independent photon density wave phase velocity with steady-state light penetration depth measurements. Instrument bandwidth and tissue absorption relaxation time ultimately determine the useful frequency range necessary for frequency-domain photon migration (FDPM) measurements.

Based on the optical properties measured in this study, we estimate that non-invasive FDPM measurements of normal uterine tissue require modulation frequencies in excess of 350 MHz.

1. Introduction

The study of light propagation in biological tissue is important in many medical and biological applications of lasers and other light sources. Absorption and scattering of light determine its spatial distribution within the irradiated tissue and the subsequent biological effects in therapeutic uses such as laser surgery (Jacques and Prahl 1987) and photodynamic therapy (Wilson and Patterson 1986). In diagnostic applications, light that is remitted, i.e. diffusely reflected from or transmitted through tissue, can be measured to probe the metabolic, physiologic or perhaps the structural status of the tissue.

From a clinical point of view, the optical properties (the absorption, μ_a, and transport scattering, μ_s', coefficients) of irradiated tissue should be determined non-invasively. This is possible using time- or frequency-domain techniques in which the perturbation of short light pulses (time-domain) or sinusoidally amplitude-modulated light waves (frequency-domain)

¶ Author to whom correspondence should be addressed.

0031-9155/94/081191+12$19.50

travelling through multiple-scattering media, such as biological tissue, are compared to the predictions of appropriate light propagation models.

In this study, the optical properties of bulk tissues were investigated using frequency-domain photon migration (FDPM) and steady-state techniques. Measurements were made in both normal and fibrotic (non-neoplastic) human uterine tissues. In all cases, the propagation of light was modelled as a diffusive process.

To our knowledge, the only previous measurements of the optical properties of human uterus were performed by Marchesini *et al* (1989) using thin (25–100 μm) frozen samples. Although such measurements have the advantage of being model independent, they are problematic due to complications associated with freezing and mechanical grinding of the tissue. These difficulties may result in measurement bias compared with the true optical property values in intact tissues. It is our estimation that techniques that employ optical biopsies of bulk, intact tissues rather than tissue biopsies will ultimately be most useful in clinical diagnostic.

2. Theory

2.1. Frequency-domain photon migration

Determination of the optical properties of multiple-scattering media, such as biological tissue, using amplitude-modulated light requires the use of an appropriate model of light propagation. In tissue optics, light propagation is commonly modelled as a diffusive process.

Only the salient features of the diffusion model will be described here. Comprehensive derivations of this model from the equation of radiative transfer have been described by several investigators including Ishimaru (1978). For measurements in biological tissue, if the source varies in time with frequencies less than 1 GHz, the diffusion equation as derived from the equation of radiative transfer is given by

$$(1/c)(\partial/\partial t)\varphi(r,t) - D\nabla^2\varphi(r,t) + \mu_a\varphi(r,t) = S(r,t) \tag{1}$$

where c is the velocity of light in the medium (it is assumed that the refractive index $n = 1.33$ for tissue-simulating phospholipid emulsions and $n = 1.40$ for tissue (Bolin *et al* 1989)), φ is the fluence rate, S is the source term for the rate of photon generation per unit volume, D is the diffusion coefficient,

$$D = [3(\mu_a + \mu_s')]^{-1} \tag{2}$$

and μ_a and μ_s' are the absorption and transport scattering coefficients respectively.

Of interest to this study are solutions to equation (1) in infinite and semi-infinite homogeneous media. In the latter case, appropriate boundary conditions must be specified in order to solve equation (1).

In frequency-domain measurements, amplitude-modulated light is launched into multiple-scattering media resulting in the propagation of diffuse photon density waves. Density wave phase lag and demodulation amplitude are measured with respect to the source response. These measurable quantities are functions of the angular modulation frequency (ω), the source–detector separation (r) and the optical properties of the medium.

2.1.1. Infinite homogeneous media. The infinite-medium solutions to equation (1) can be expressed in terms of the measured parameters phase (ϕ) and demodulation (m) (Tromberg *et al* 1993)

$$\phi = k_i r \tag{3}$$

and

$$m = \exp[-(k_r - 1/\delta)] \tag{4}$$

where k_i and k_r are, respectively, the imaginary and real components of the complex photon density wave number:

$$k_i = (\tfrac{3}{2}\mu_a(\mu_a + \mu_s'))^{1/2}((1 + (\omega/\mu_a c)^2)^{1/2} - 1)^{1/2} \tag{5}$$

and

$$k_r = (\tfrac{3}{2}\mu_a(\mu_a + \mu_s'))^{1/2}((1 + (\omega/\mu_a c)^2)^{1/2} + 1)^{1/2}. \tag{6}$$

ω and δ are the angular frequency and DC penetration depth, respectively. The penetration depth is given by

$$\delta = [3\mu_a(\mu_a + \mu_s')]^{-1/2}. \tag{7}$$

The photon density wave phase velocity ($V_p = \omega/k_i$) reaches a dispersionless lower limit independent of modulation frequency when $\omega \ll \mu_a c$. Under these conditions, photon density wave attenuation is dominated by absorption and V_p can be expressed in terms of the penetration depth (Tromberg *et al* 1993)

$$V_p = 2\mu_a c\delta. \tag{8}$$

If the source and detector fibres are separated by a sufficient distance such that diffusion theory is valid, the fluence rate (φ) will decay exponentially with source–detector separation

$$\varphi(r) = \varphi_0/r \exp(-r/\delta) \tag{9}$$

where φ_0 is the fluence rate at some initial separation. Thus a plot of $\ln[\varphi_0/r\varphi(r)]$ against r yields a straight line with slope $1/\delta$.

The phase velocity and phase slope (the slope of the phase against frequency plot) are related by (Tromberg *et al* 1993)

$$\alpha = r/V_p \tag{10}$$

where α is the phase slope. Thus measurements of the phase slope as a function of fibre separation yields V_p.

2.1.2. Semi-infinite homogeneous media. The solutions to equation (1) in a semi-infinite medium using a unified partial current/extrapolated boundary condition (Haskell *et al* 1994) are given by

$$\phi = k_i r_0 - \tan^{-1}(\text{imag/real}) \tag{11}$$

and

$$m = (\text{real}^2 + \text{imag}^2)^{1/2}/dc \tag{12}$$

where the real and imaginary components of the solution are

$$\text{real} = \exp(-k_r r_0)/r_0 - \cos[k_i(r_{0b} - r_0)]\exp(-k_r r_{0b})/r_{0b} \tag{13}$$

$$\text{imag} = \sin[k_i(r_{0b} - r_0)]\exp(-k_r r_{0b})/r_{0b} \tag{14}$$

$$dc = \exp(-r_0/\delta)/r_0 - \exp(-r_{0b}/\delta)/r_{0b} \tag{15}$$

$$r_0 = (r^2 + (\mu_a + \mu_s')^{-2})^{1/2} \qquad r_{0b} = (r^2 + (2z_b + (\mu_a + \mu_s')^{-1})^2)^{1/2}$$

$$z_b = [(1 + R_{\text{eff}})/(1 - R_{\text{eff}})]\tfrac{2}{3}(\mu_a + \mu_s')^{-1}$$

and

$$R_{\text{eff}} = \begin{cases} 0.431 & n = 1.33 \\ 0.493 & n = 1.40. \end{cases}$$

The terms dc, r, z_b and R_{eff} are the time-independent component of the source term, the source–detector separation, the distance between the real and extrapolated boundaries and the effective reflection coefficient, respectively. A complete description of photon density wave behaviour at an air/tissue boundary has been presented elsewhere (Svaasand *et al* 1993, Haskell *et al* 1994).

3. Materials and methods

3.1. Instrumentation

The photon migration instrument used in these experiments (figure 1) has been described extensively elsewhere (Tromberg *et al* 1993). Briefly, an argon-ion laser (Innova 90-5, Coherent, Palo Alto, CA, USA) is used to pump a dye laser (Coherent model 599) containing DCM dye (Exciton, Inc., Dayton, OH, USA). High-harmonic-content pulses are produced by passing the light through a Pockels cell (PC) driven by the amplified output of a harmonic comb generator (HGG1). In the frequency domain, the comb generator outputs consist of a fundamental frequency (5 MHz) and its integer harmonics, 10, 15, 20 MHz, etc. The resultant pulses are focused onto a flat-cut 600 μm diameter fused silica fibre (F1), which is used to direct light into the sample. A small portion of this light is diverted to a reference

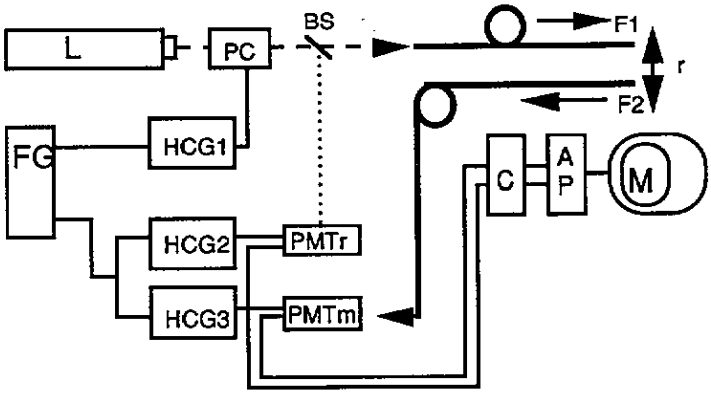

Figure 1. The frequency-domain instrument: BS, beam splitter; M, display monitor; L, laser; FG, frequency generator.

photomultiplier tube (PMT_r) (Hamamatsu R928), which allows phase and modulation locking of the instrument.

Scattered light is collected by a second fibre (F2) identical to F1 and transmitted to the measurement photomultiplier tube (PMT_m) (Hamamatsu R928). The gain of the detectors is modulated by HCG2 and HCG3 at a small frequency offset (3 Hz) from that of the modulated excitation. Since the outputs of these devices are the harmonic combs, 5 MHz + 3 Hz, 10 MHz + 6 Hz, 15 MHz + 9 Hz, ..., 250 MHz + 150 Hz, the sample's phase and amplitude response at each harmonic is contained within the cross-correlation frequencies 3, 6, 9 Hz, etc. These 3 Hz frequencies are sampled and digitized by a dual-channel analogue-to-digital converter (C). The digital data are converted to a frequency spectrum by an array processor (AP). Phase and modulation data can be acquired from 50 frequencies up to 250 MHz in less than 1 s. Typical tissue measurements are integrated for about 30 s in order to achieve reasonable signal to noise over the entire frequency spectrum.

3.2. Solution measurements

In order to determine the validity of the semi-infinite model (equation (11) and (12)), measurements were conducted in a 4 l cylindrical glass beaker containing a turbid solution of known optical properties—1.19 μg ml^{-1} of nickel tetrasulphonated phthalocyanine (NiSPC) (Mid-Century Pharmaceuticals, IL, USA) and 3.5 l of 2% Intralipid (Kabivitrum, Inc., Clayton, NC, USA). The source and detector fibres were placed at the surface of the solution in the centre of the beaker. The source–detector separation was varied from 5 to 20 mm. Prior to the sample measurements, a reference measurement was recorded in air with the source and detector fibres abutted. A wavelength of 650 nm was chosen to coincide with the absorption peak of nickel phthalocyanine. The analytical expressions for phase (equation (11)) and modulation (equation (12)) were fitted to the experimental data using a grid-search chi-square fitting routine (Bevington 1969).

3.3. Uterus measurements

Intact uteri were obtained immediately following hysterectomy and placed on ice. *Ex vivo* measurements were performed on six cold, fresh specimens (one post- and five pre-menopausal). During the measurement period (typically 3–4 h), wet gauze was applied

to the uterus to prevent dehydration. Samples were returned to the pathologist for tissue analysis upon completion of the measurements. In all cases, a wavelength of 630 nm was used to coincide with the absorption peak of Photofrin II—a commonly used photosensitizer in photodynamic therapy (PDT).

3.3.1. Reflectance measurements. For a representative uterus, non-invasive reflectance measurements (both source and detector fibre on the surface of the uterus) were attempted on both normal and fibrotic tissues. In each case, measurements were made at three or four source–detector separations ranging from 5 to 20 mm. Measurements were repeated five times at each source–detector location. The optical properties were determined by fitting the semi-infinite expressions (equations (11) and (12)) to the data using the chi-square fitting routine described previously.

3.3.2. Transmittance measurements. In all samples investigated, both frequency-domain and steady-state measurements were performed in transmittance mode, i.e. with source and detector fibres inserted into the tissue facing each other. Small-gauge needles were used to bore channels into the tissue so that source and detector fibres could be inserted without mechanical shearing. The source fibre was inserted approximately 10 mm into the uterus while the detector fibre was inserted from the opposite side until it was approximately 5 mm from the source.

In the case of frequency–domain measurements, phase and modulation were recorded as a function of source–detector separation by backing the detector fibre away from the source using a micropositioner. In all cases, the detector fibre was never closer than 10 mm from the nearest surface. Measurements were repeated five times for each source–detector position. In order to avoid uncertainties associated with tissue relaxation as the detector fibre was retracted, a period of 30 s was observed at each position before recording the data. The optical properties were determined by fitting the infinite-medium expressions (equations (3) and (4)) to the data. While the detector fibre was oriented so that it received both the flux and fluence terms in the radiance, the flux contribution was determined to be negligible.

In the steady-state measurements, the light beam was steered around the Pockels cell and launched directly into the source fibre. The DC intensity was then recorded as a function of source–detector separation. The detector fibre was moved in increments of either 1 or 2 mm and three measurements were made at each source–detector separation.

4. Results and discussions

The frequency dependences of the phase and modulation in 2% Intralipid are illustrated in figure 2(a) and (b), respectively. The smooth curves through the data represent the best non-linear least-squares fits to equations (11) and (12). The phase is linear over a substantial frequency range (up to about 150 MHz) and the modulation decreases sufficiently (0.9 at 180 MHz) to allow accurate determination of the optical properties. The fitted absorption coefficient ($1.12 \pm 0.14 \times 10^{-2}$ mm^{-1}) was found to be in good agreement with that expected based on the absorption of NISPC at 650 nm ($9.7 \pm 0.1 \times 10^{-3}$ mm^{-1}). The fitted transport scattering coefficient (2.64 ± 0.32 mm^{-1}) was in good agreement with the theoretical value (2.50 ± 0.12 mm^{-1}) calculated from Mie theory (van Staveren *et al* 1991). Typical reduced chi-square values obtained in these experiments ranged from 0.8 to 1.2.

Figure 3(a) and (b) illustrates typical phase and modulation results, respectively, obtained in a large fibroid. Measurements were made in both semi-infinite (source and detector fibres

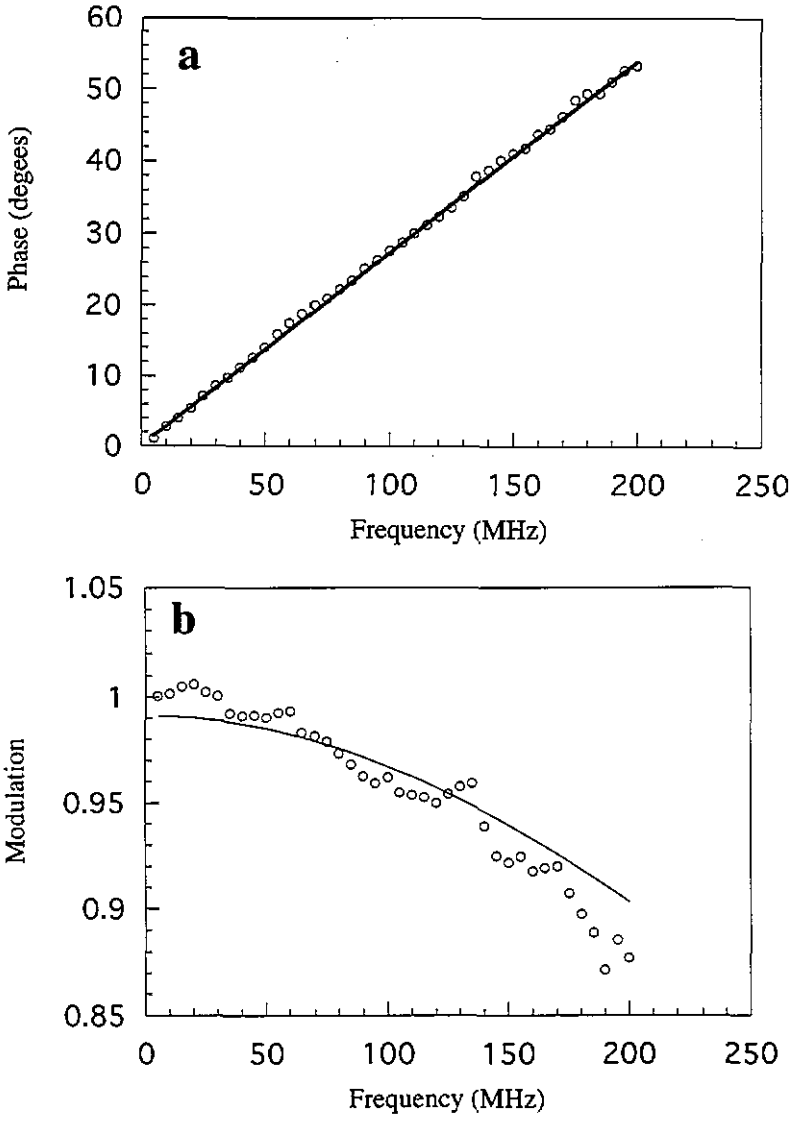

Figure 2. The phase (a) and modulation (b) versus frequency response for 2% Intralipid and 1.19 μg ml^{-1} of NiSPC absorber. The smooth curves through the data represent the best non-linear least-squares fits to (11) and (12); $\lambda = 650$ mm and $r = 16$ mm.

located at the surface) and infinite (both fibres embedded in the tissue) geometries. The lines through the data represent the best non-linear least-square fits to equations (3) and (4) in the infinite geometry and equations (11) and (12) in the semi-finite case. The fitting algorithm was structured such that both phase and modulation were fitted simultaneously. The phase results show good agreement between the model (equations (3) and (11)) and the data in both geometries. The modulation data were noisier and thus the fits to equations (4) and (12) were not as good. For the frequency range shown, the decrease in modulation (10%–15%) was substantially greater than what we observed in normal uterine tissue

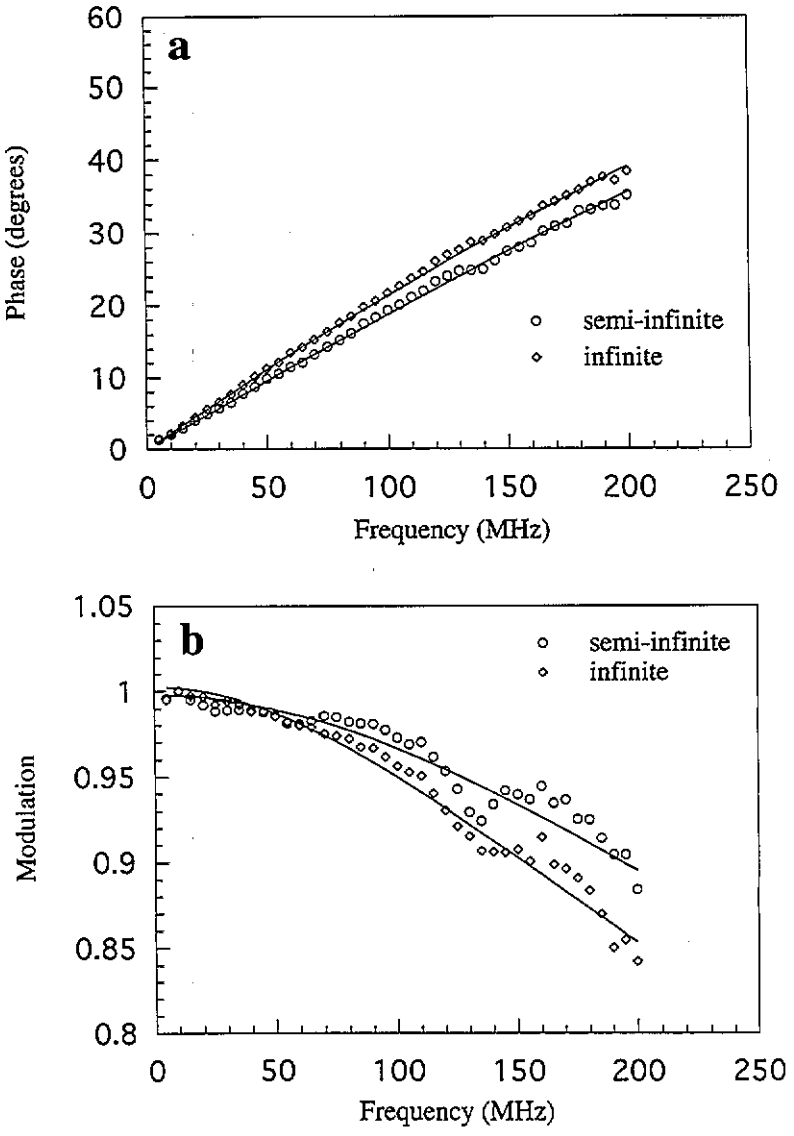

Figure 3. Phase (a) and modulation (b) versus frequency response for a large fibroid. The smooth curves through the date represent the best non-linear least-squres fits to (11) and (12) in the semi-infinite case and (3) and (4) in the infinite geometry; $\lambda = 630$ nm and $r = 14$ mm.

(typically 5%). This was attributed to the fact that the absorption of the fibroid was much lower than that of normal tissue. The fitted optical properties obtained in the infinite geometry ($\mu_a = 3.0 \pm 0.3 \times 10^{-3}$ mm^{-1} and $\mu_s' = 0.60 \pm 0.06$ mm^{-1}) were in good agreement with those obtained in the semi-finite case ($\mu_a = 3.3 \pm 0.3 \times 10^{-3}$ mm^{-1} and $\mu_s' = 0.75 \pm 0.08$ mm^{-1}).

Attempts to obtain values for μ_a and μ_s' in normal, non-fibrotic uteri using the full fit procedure (fitting to both the phase and modulation simultaneously) resulted in ambiguities in the fitted optical properties, i.e. repeated measurements at a given fibre separation yielded

values that typically differed by a factor of five or more. This was attributed to high tissue absorption. As absorption increases, the demodulation and phase slopes become smaller and more linear. The poor quality of the fitted optical properties are reflected by reduced chi-square values, which were either too low (typically less than 0.5) or too high (typically greater than 5.0).

In order to determine accurately the optical properties of the uterines tissues, infinite-geometry measurements of phase and steady-state penetration depth were combined. Results of the phase slope against source–detector fibre separation for a typical pre-menopausal uterus sample are illustrated in figure 4. Each data point represents the mean of five phase against frequency slope calculations. The solid line is a linear fit to the data. The low-frequency cut-off for the determination of the phase slope was based on the best linear fit to the phase against frequency data as judged by the correlation coefficient. Typically, this cut-off ranged from 90 to 130 MHz. The phase velocity can be extracted from the reciprocal slope of this plot (equation (10)). As expected, these results indicate that the phase velocity is frequency independent and constant over these distances and frequencies.

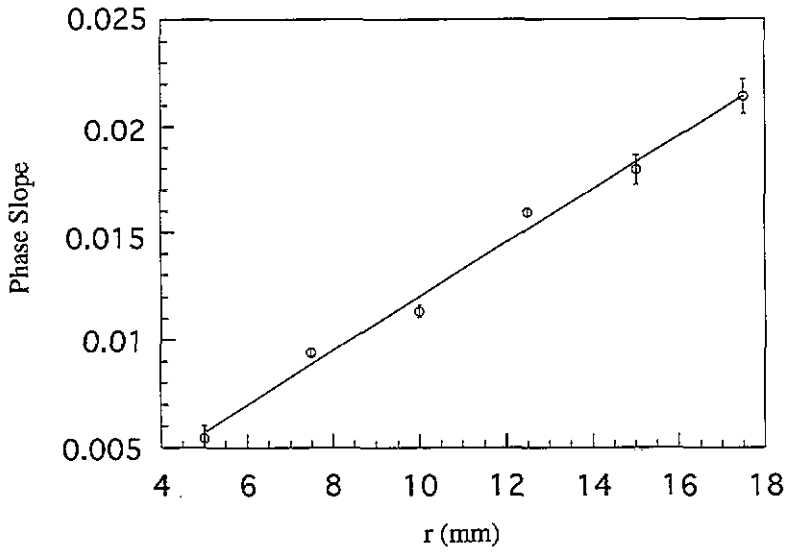

Figure 4. The phase slope against source–detector fibre separation for a pre-menopausal uterus. The line represents a linear fit to the data.

Results of the steady-state penetration-depth measurements in the same pre-menopausal uterus are illustrated in figure 5. The penetration depth was determined from the slope of the best-fit line according to equation (9). The optical properties of the bulk uterus were then determined based on the phase-velocity and penetration-depth measurements (equation (7)). The results are summarized in table 1. The samples have been divided into three categories: post-menopausal, pre-menopausal and fibrotic tissues. There appear to be significant differences in the penetration depth, phase velocity and absorption coefficient between the three different tissue types. The penetration depth should decrease with increasing absorption (equation (7)) while the phase velocity should increase (equation (8)). This is in good agreement with the results shown in table 1, i.e. the sample with the highest

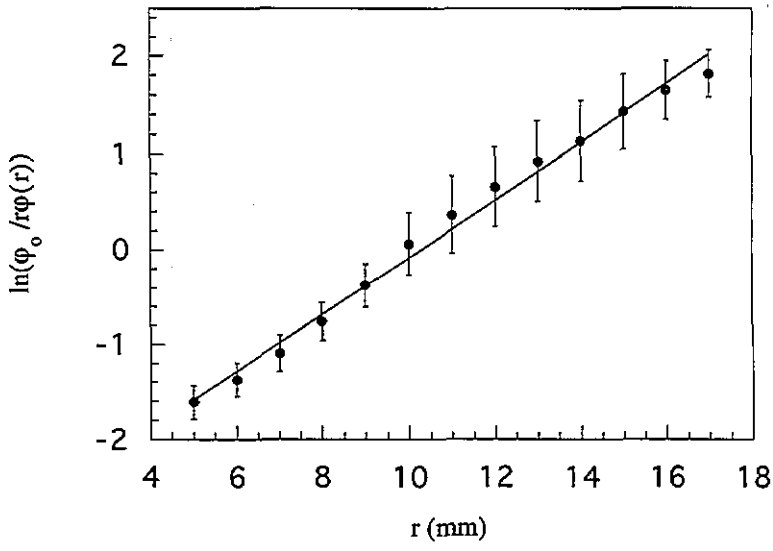

Figure 5. Steady-state penetration depth measurements for a pre-menopausal uterus. The linear fit to the data is denoted by the line.

Table 1. Optical parameters of the uterus.

Sample	No of samples	Penetration depth (mm)	Phase velocity (mm s^{-1})	Absorption coefficient (mm^{-1})	Scattering coefficient (mm^{-1})
Post-menopausal	1	2.59 ± 0.26	$(5.72 \pm 0.17) \times 10^{10}$	$(5.15 \pm 0.54) \times 10^{-2}$	0.91 ± 0.17
Pre-menopausal	4	4.79 ± 0.32	$(3.96 \pm 0.07) \times 10^{10}$	$(1.93 \pm 0.13) \times 10^{-2}$	0.73 ± 0.09
		3.39 ± 0.28	$(4.56 \pm 0.22) \times 10^{10}$	$(3.14 \pm 0.30) \times 10^{-2}$	0.89 ± 0.15
		5.11 ± 0.20	$(4.65 \pm 0.49) \times 10^{10}$	$(2.13 \pm 0.24) \times 10^{-2}$	0.60 ± 0.08
		4.77 ± 0.45	$(4.02 \pm 0.49) \times 10^{10}$	$(1.97 \pm 0.30) \times 10^{-2}$	0.73 ± 0.15
Fibroid	1	7.46 ± 0.43	$(2.63 \pm 0.18) \times 10^{10}$	$(8.24 \pm 0.75) \times 10^{-3}$	0.72 ± 0.09

absorption had the smallest penetration depth and the highest phase velocity. Conversely, the lowest-absorbing tissue had the highest penetration depth and the smallest phase velocity.

Absorption differences between the three tissue types were probably due to differences in water and haemoglobin content. For example, post menopausal uterus absorption may have been a consequence of its small size, reduced water content and relatively high blood volume. In contrast, the low fibroid absorption is consistent with its poor vascularity. No significant differences in the transport scattering coefficients were observed, although the dense, shrunken post-menopausal uterus had slightly higher μ_s' values than some of the pre-menopausal and fibroid samples. This is consistent with the fact that post-menopausal tissue is predominantly muscle. We are currently comparing the size and density of cells in each sample using conventional histological techniques.

Inter-sample variations may be due to differences in the stage of the menstrual cycle at which the measurements were made. The uterus is under hormonal control and undergoes significant morphological change (including blood content) during the cycle. Unfortunately, the stage of the menstrual cycle was not known since the surgeon does not record this prior to hysterectomy.

The absorption coefficients of normal uteri obtained in this study are in good agreement with the results of Marchesini *et al* (1989) (0.035 mm^{-1} at 635 nm); however, their transport scattering coefficient is much higher (12.2 mm^{-1}) than those measured here. As a result, the penetration depths obtained in this study are somewhat higher than that calculated from the optical properties obtained by Marchesini *et al* (1989) (0.88 mm). This discrepancy is probably due to the fact that the measurements described here were performed on fresh hydrated bulk samples, whereas the measurements of Marchesini *et al* (1989) were performed on thin tissue sections, which are susceptible to dehydration. As tissues become dehydrated, the tissue volume fraction increases, resulting in increased scattering and a subsequent decrease in the penetration depth.

In principle it should be possible to obtain the optical properties of uterine tissues non-invasively using only phase and modulation information. However, due to the limited frequency range of the instrument (up to 250 MHz), we were unable to use the phase and modulation to reliably calculate the optical properties of highly absorbing normal uterine tissues. The minimum frequency required for accurate measurements is a complex function of the sample optical properties and source–detector separation. Patterson (1994) has developed an expression that characterizes the relationship between these parameters:

$$f > \left[c^2\mu_a/5\pi^2 r\sqrt{3/(1-\alpha')}\right]^{1/2} \tag{16}$$

where α' is reduced albedo ($\mu_s'/(\mu_s'+\mu_a)$). For example, for typical normal uterine tissues ($\mu_a = 0.02$ mm^{-1}, $\mu_s' = 0.7$ mm^{-1}) and $r = 14$ mm, f should be greater than 357 MHz. Given the optical properties of the fibroid from table 1 and $r = 14$ mm, f should be greater than 183 MHz. Although our equipment has an upper frequency limit of 250 MHz, data above 200 MHz are usually very noisy and are often excluded from the analysis. Thus, in the case of fibrotic tissue, the useful frequency range is extremely narrow (180–200 MHz). Furthermore, at 200 MHz, the demodulation (approximately 10%) is very close to the noise limit. Thus, with only a limited number of noisy data points, one would not expect to obtain reliable estimates of the optical properties. This would explain the discrepancy between fibroid absorption determined by frequency-domain (figure 3(a) and (b)) and combined (table 1) techniques.

We estimate that modulation frequencies up to 500 MHz are required in order to reliably calculate optical properties solely from phase and modulation information. Compensating for the limited frequency range of our instrument by increasing r was not possible due to poor signal-to-noise ratios beyond 15 mm. Given the limitations of our frequency-domain apparatus, we believe that the most reliable technique for determining tissue optical properties involves combining phase velocity and penetration depth information.

5. Conclusions

The results presented here were obtained using a relatively small sample size; however, sample precision was extremely high. We thus suspect that the optical property differences observed were real. A larger sample size is required in order to determine whether all uteri fall within the range of optical properties measured in this study.

Using combined steady-state and frequency-domain techniques, the absorption coefficient of normal post-menopausal human uterine tissues ($\sim$ 0.06 mm^{-1}) was found to be significantly greater than that of normal pre-menopausal tissue (0.02–0.03 mm^{-1}) and pre-menopausal fibrotic tissue ($\sim$ 0.008 mm^{-1}). Differences in absorption were attributed

to differences in water and haemoglobin content. The transport scattering coefficient of the post-menopausal sample (0.91 mm^{-1}) was slightly higher than those of the pre-menopausal samples (0.60–0.90 mm^{-1}); however, the normal and fibrotic pre-menopausal samples were found to have similar values.

Full fits utilizing both phase and modulation against frequency information are possible in fibrotic tissue due to low absorption. However, fitted absorption coefficients were approximately three times lower than those obtained using the combined steady-state and frequency-domain technique. The origin of this discrepancy was attributed primarily to noise in the frequency-domain demodulation data. High absorption in normal uterine tissues similarly restricted our ability to calculate optical properties from phase and modulation data. However, reliable estimates of the optical properties were obtained from high-precision phase-slope and DC penetration-depth measurements. Finally, we expect that modulation frequencies greater than 350 MHz are required in order to non-invasively obtain optical properties of such highly absorbing tissues using only non-invasive FDPM techniques.

Acknowledgments

This work was supported by the Whitaker Foundation (WF16493), the National Institutes of Health (R29GM50958) and Beckman Instruments Inc. In addition, we acknowledge program support from the Office of Naval Research (N00014-91-0134), the Department of Energy (DE-FG-3-91-ER61227) and the National Institutes of Health (5P41RR01192-15). The authors are grateful to Eric Cho, David Pham, Cuong Ly and Tuan Ho for their assistance.

References

Bevington P R 1969 *Data Reduction and Error Analysis for the Physical Sciences* (New York: McGraw-Hill)

Bolin F P, Preuss L E, Taylor R C and Ference R J 1989 Refractive index of some mammalian tissues using a fiber optic cladding method *Appl. Opt.* **28** 2297–303

Haskell R C, Svaasand L O, Tsay T-T, Feng T-C, McAdams M S and Tromberg B J *J. Opt. Soc. Am.* A at press

Ishimaru A 1978 *Wave Propagation and Scattering in Random Media* vol 1 (New York: Academic)

Jaques S L and Prahl S A 1987 Modeling optical and thermal distributions in tissue during laser irradiation *Lasers Surg. Med.* **6** 494–503

Marchesini R, Bertoni A, Andreola S, Melloni E and Sichirollo A E 1989 Extinction and absorption coefficients and scattering phase functions of human tissues *in vitro Appl. Opt.* **28** 2318–24

Patterson M S 1994 Principles and applications of frequency domain measurements of light propagation *Optical and Thermal Response of Laser Irradiated Tissue* ed A J Welch and M J C van Gemert (New York: Plenum) at press

Svaasand L O, Tromberg B J, Haskell R C, Tsey T-T and Berns M W 1993 Tissue characterization and imaging using photon density waves *Opt. Eng.* **32** 258–66

Tromberg B J, Svaasand L O, Tsay T T and Haskell R C 1993 Properties of photon density waves in multiple scattering media *Appl. Opt.* **32** 607–16

van Staveren H J, Moes C J M, van Marle J, Prahl S A and van Gemert M J C 1991 Light scattering in Intralipid-10% in the wavelength range 400–1100 nm *Appl. Opt.* **30** 4507–14

Wilson B C and Patterson M S 1986 The physics of photodynamic therapy *Phys. Med. Biol.* **31** 327–60